The Astrophysical Journal Letters, 1003:L47 (11pp), 2026 June 1 https://doi.org/10.3847/2041-8213/ae6780

A Natural $\gtrsim$100× Telescope: Discovery of the Strongly Lensed Type II SN 2025mkn at $z = 1.37$

Cameron Lemon[1], Ariel Goobar[1], Joel Johansson[1], Edvard Mörtsell[1], Steve Schulze[2], Igor Andreoni[3], Aleksandra Bochenek[4], Seán J. Brennan[5], Malte Busmann[6,7], Michael Coughlin[8], Kaustav K. Das[9], Suhail Dhawan[10], Christoffer Fremling[11,12], Anjasha Gangopadhyay[13], Daniel Gruen[6,7], Xander J. Hall[14], Anna Y. Q. Ho[15], Mansi M. Kasliwal[11], Daniel A. Perley[4], Mickael Rigault[16], Genevieve Schroeder[15], Mathew Smith[17], Jesper Sollerman[13], Jean J. Somalwar[18,19], Robert Stein[20,21,22], Stephen Thorp[1,23], Alice Townsend[24], Jacob L. Wise[4], Lin Yan[12], Nikki Arendse[1], Eric C. Bellm[25], Tracy X. Chen[26], Andrew Drake[9], Frank J. Masci[26], Josiah Purdum[12], Roger Smith[12], Jason T. Hinkle[27,28,71], T. Emil Rivera-Thorsen[13], Benjamin J. Shappee[29], Michael A. Tucker[30,72], Jessica Aguilar[31], Steven Ahlen[32], Greg Aldering[31], Segev BenZvi[33], Davide Bianchi[34,35], David Brooks[36], Todd Claybaugh[31], Axel de la Macorra[37], John Della Costa[38,39], Arjun Dey[39], Peter Doel[36], Brenna Flaugher[40], Andreu Font-Ribera[41,42], Jaime E. Forero-Romero[43,44], Enrique Gaztañaga[45,46,47], Satya Gontcho A. Gontcho[48], Gaston Gutierrez[40], Dragan Huterer[49,50], Mustapha Ishak[51], Jorge Jimenez[42], Dick Joyce[39], Stephanie Juneau[39], Robert Kehoe[52], Alex G. Kim[53], David Kirkby[53], Theodore Kisner[31], Anthony Kremin[31], Ofer Lahav[36], Martin Landriau[31], Laurent Le Guillou[54], Michael E. Levi[31], Marc Manera[42,55], Aaron Meisner[39], Ramon Miquel[41,42], John Moustakas[56], Seshadri Nadathur[46], Brendan O'Connor[57], Nathalie Palanque-Delabrouille[31,58], Antonella Palmese[57], Will J. Percival[59,60,61], Ignasi Pérez-Ràfols[62], Claire Poppett[31,63,64], Francisco Prada[65], Graziano Rossi[66], Eusebio Sanchez[67], David Schlegel[31], Michael Schubnell[49,50], Arman Shafieloo[68,69], Joseph Silber[31], David Sprayberry[39], Gregory Tarlé[50], Benjamin A. Weaver[39], and Hu Zou[70]

[1] Department of Physics, Oskar Klein Centre, Stockholm University, SE-106 91, Stockholm, Sweden; ariel@fysik.su.se
[2] Center for Interdisciplinary Exploration and Research in Astrophysics (CIERA), Northwestern University, 1800 Sherman Ave., Evanston, IL 60201, USA
[3] Department of Physics and Astronomy, University of North Carolina, 120 East Cameron Ave., Chapel Hill, NC 27599, USA
[4] Astrophysics Research Institute, Liverpool John Moores University, 146 Brownlow Hill, Liverpool L3 5RF, UK
[5] Max-Planck-Institut für Astrophysik, Karl-Schwarzschild-Straße 1, D-85748 Garching, Germany
[6] University Observatory, Faculty of Physics, Ludwig-Maximilians-Universität, Scheinerstr. 1, 81679 Munich, Germany
[7] Excellence Cluster ORIGINS, Boltzmannstr. 2, 85748 Garching, Germany
[8] School of Physics and Astronomy, University of Minnesota, Minneapolis, MN 55455, USA
[9] Cahill Center for Astrophysics, California Institute of Technology, 1200 E. California Blvd., Pasadena, CA 91125, USA
[10] Birmingham Institute for Gravitational Wave Astronomy and School of Physics and Astronomy, University of Birmingham, Birmingham B15 2TT, UK
[11] Division of Physics, Mathematics and Astronomy, California Institute of Technology, Pasadena, CA 91125, USA
[12] Caltech Optical Observatories, California Institute of Technology, Pasadena, CA 91125, USA
[13] Department of Astronomy, Oskar Klein Center, Stockholm University, SE-106 91 Stockholm, Sweden
[14] McWilliams Center for Cosmology and Astrophysics, Department of Physics, Carnegie Mellon University, 5000 Forbes Ave., Pittsburgh, PA 15213, USA
[15] Department of Astronomy, Cornell University, Ithaca, NY 14853, USA
[16] Universite Claude Bernard Lyon 1, CNRS, IP2I Lyon / IN2P3, IMR 5822, F-69622 Villeurbanne, France
[17] Department of Physics, Lancaster University, Lancashire, LA1 4YB, UK
[18] Department of Astronomy, University of California, Berkeley, CA 94720-3411, USA
[19] Kavli Institute for Particle Astrophysics and Cosmology, Stanford, CA 94305, USA
[20] Department of Astronomy, University of Maryland, College Park, MD 20742, USA
[21] Joint Space-Science Institute, University of Maryland, College Park, MD 20742, USA
[22] Astrophysics Science Division, NASA Goddard Space Flight Center, Mail Code 661, Greenbelt, MD 20771, USA
[23] Institute of Astronomy and Kavli Institute for Cosmology, University of Cambridge, Madingley Road, Cambridge, CB3 0HA, UK
[24] Institut für Physik, Humboldt-Universität zu Berlin, Newtonstr. 15, 12489 Berlin, Germany
[25] DIRAC Institute, Department of Astronomy, University of Washington, 3910 15th Ave. NE, Seattle, WA 98195, USA
[26] IPAC, California Institute of Technology, 1200 E. California Blvd., Pasadena, CA 91125, USA
[27] Department of Astronomy, University of Illinois Urbana-Champaign, 1002 West Green St., Urbana, IL 61801, USA
[28] NSF-Simons AI Institute for the Sky (SkAI), 172 E. Chestnut St., Chicago, IL 60611, USA
[29] Institute for Astronomy, University of Hawai'i, 2680 Woodlawn Drive, Honolulu, HI 96822-1839, USA
[30] Center for Cosmology and Astroparticle Physics, The Ohio State University, 191 West Woodruff Ave., Columbus, OH 43215, USA
[31] Lawrence Berkeley National Laboratory, 1 Cyclotron Road, Berkeley, CA 94720, USA
[32] Department of Physics, Boston University, 590 Commonwealth Ave., Boston, MA 02215, USA
[33] Department of Physics & Astronomy, University of Rochester, 206 Bausch and Lomb Hall, P.O. Box 270171, Rochester, NY 14627-0171, USA
[34] Dipartimento di Fisica "Aldo Pontremoli," Università degli Studi di Milano, Via Celoria 16, I-20133 Milano, Italy
[35] INAF-Osservatorio Astronomico di Brera, Via Brera 28, 20122 Milano, Italy
[36] Department of Physics & Astronomy, University College London, Gower St., London, WC1E 6BT, UK
[37] Instituto de Física, Universidad Nacional Autónoma de México, Circuito de la Investigación Científica, Ciudad Universitaria, Cd. de México C. P. 04510, Mexico
[38] Department of Astronomy, San Diego State University, 5500 Campanile Drive, San Diego, CA 92182, USA
[39] NSF NOIRLab, 950 N. Cherry Ave., Tucson, AZ 85719, USA
[40] Fermi National Accelerator Laboratory, PO Box 500, Batavia, IL 60510, USA
[41] Institució Catalana de Recerca i Estudis Avançats, Passeig de Lluís Companys, 23, 08010 Barcelona, Spain
[42] Institut de Física d'Altes Energies (IFAE), The Barcelona Institute of Science and Technology, Edifici Cn, Campus UAB, 08193, Bellaterra (Barcelona), Spain
[43] Departamento de Física, Universidad de los Andes, Cra. 1 No. 18A-10, Edificio Ip, CP 111711, Bogotá, Colombia
[44] Observatorio Astronómico, Universidad de los Andes, Cra. 1 No. 18A-10, Edificio H, CP 111711, Bogotá, Colombia
[45] Institut d'Estudis Espacials de Catalunya (IEEC), E-08034 Barcelona, Spain

[46] Institute of Cosmology and Gravitation, University of Portsmouth, Dennis Sciama Building, Burnaby Road, Portsmouth PO1 3FX, UK
[47] Institute of Space Sciences (ICE, CSIC), Campus UAB, Carrer de Can Magrans, s/n, E-08193 Barcelona, Spain
[48] Department of Astronomy, University of Virginia, 530 McCormick Rd, Charlottesville, VA 22904, USA
[49] Department of Physics, University of Michigan, 450 Church St., Ann Arbor, MI 48109, USA
[50] University of Michigan, 500 Sout State St., Ann Arbor, MI 48109, USA
[51] Department of Physics, The University of Texas at Dallas, 800 W. Campbell Rd., Richardson, TX 75080, USA
[52] Department of Physics, Southern Methodist University, 3215 Daniel Ave., Dallas, TX 75275, USA
[53] Department of Physics and Astronomy, University of California, Irvine, 92697, USA
[54] Sorbonne Université, CNRS/IN2P3, Laboratoire de Physique Nucléaire et de Hautes Energies (LPNHE), FR-75005 Paris, France
[55] Departament de Física, Serra Húnter, Universitat Autònoma de Barcelona, 08193, Bellaterra (Barcelona), Spain
[56] Department of Physics and Astronomy, Siena University, 515 Loudon Road, Loudonville, NY 12211, USA
[57] Department of Physics, Carnegie Mellon University, 5000 Forbes Ave., Pittsburgh, PA 15213-3815, USA
[58] IRFU, CEA, Université Paris-Saclay, F-91191 Gif-sur-Yvette, France
[59] Department of Physics and Astronomy, University of Waterloo, 200 University Ave. W, Waterloo, ON N2L 3G1, Canada
[60] Perimeter Institute for Theoretical Physics, 31 Caroline St. N., Waterloo, ON N2L 2Y5, Canada
[61] Waterloo Centre for Astrophysics, University of Waterloo, 200 University Ave. W, Waterloo, ON N2L 3G1, Canada
[62] Departament de Física, EEBE, Universitat Politècnica de Catalunya, c/Eduard Maristany 10, 08930 Barcelona, Spain
[63] Space Sciences Laboratory, University of California, Berkeley, 7 Gauss Way, Berkeley, CA 94720, USA
[64] University of California, Berkeley, 110 Sproul Hall #5800, Berkeley, CA 94720, USA
[65] Instituto de Astrofísica de Andalucía (CSIC), Glorieta de la Astronomía, s/n, E-18008 Granada, Spain
[66] Department of Physics and Astronomy, Sejong University, 209 Neungdong-ro, Gwangjin-gu, Seoul 05006, Republic of Korea
[67] CIEMAT, Avenida Complutense 40, E-28040 Madrid, Spain
[68] Korea Astronomy and Space Science Institute, 776, Daedeokdae-ro, Yuseong-gu, Daejeon 34055, Republic of Korea
[69] University of Science and Technology, 217 Gajeong-ro, Yuseong-gu, Daejeon 34113, Republic of Korea
[70] National Astronomical Observatories, Chinese Academy of Sciences, A20 Datun Road, Chaoyang District, Beijing 100101, People's Republic of China
Received 2026 February 18; revised 2026 April 9; accepted 2026 April 20; published 2026 May 29

Abstract

We present the discovery of SN 2025mkn, a gravitationally lensed Type II supernova. First detected as a blue transient in Zwicky Transient Facility (ZTF), 0.″83 from a $z = 0.42$ elliptical galaxy, the follow-up SNIFS/UH2.2 m and LRIS/Keck spectra revealed absorption lines at $z = 1.371$. Later JWST NIRCam imaging shows that the bright transient is a close pair of point sources separated by ∼0.″07, and a 30 times fainter counterimage opposite the lens, for which NIRSpec reveals strong Hα emission also at $z = 1.371$. The lightcurves and spectra are consistent with the Type II supernova source being magnified $\gtrsim$100 times, with ∼250 required to reconcile its luminosity with that of nearby events such as SN 2023ixf. Lens models are consistent with such high magnifications, and always show that the faint image arrived first (undetected in earlier ZTF imaging), consistent with the later spectral phase of this fainter image. A fourth image is also predicted and possibly detected in the NIRSpec data. Lightcurve-based time-delay measurements are not possible due to the first image being the faintest; however, the resolved NIRSpec spectra offer a future opportunity for time-delay cosmography through supernova phase measurements.

Unified Astronomy Thesaurus concepts: Strong gravitational lensing (1643); Type II supernovae (1731); Supernovae (1668)

1. Introduction

Strong gravitational lenses are unique astrophysical tools: they allow direct probes of total masses within the Einstein radius (e.g., A. J. Shajib et al. 2024), reach resolutions impossible for unlensed sources thanks to the associated magnification (e.g., parsec scales at $z = 2$, E. Vanzella et al. 2022), and provide multiple subkiloparsec lines of sight to study spatial variations in kinematics and chemistry in galaxies (e.g., S. Cristiani et al. 2024), among many other uses. Nearly all strong lens systems discovered to date have galaxy or quasar sources (C. Lemon et al. 2024), the latter of which are time variable, opening up additional science cases such as microlensing studies to probe compact matter fractions in lensing galaxies (e.g., G. Vernardos et al. 2024), and time-delay cosmography, in which the time delays between image pairs are measured and used to constrain the Hubble constant (S. Refsdal 1964). For the latter application, S. Refsdal (1964) originally proposed supernova sources, but only in recent years have such systems been discovered (R. M. Quimby et al. 2013; P. L. Kelly et al. 2015; A. Goobar et al. 2017). These lensed supernovae (SNe), despite only providing time-domain information during the lifetime of the supernova, offer several advantages over lensed quasars: (i) time-delay measurements are often easier due to the known shape of the supernova lightcurve; (ii) time delays can be measured independently from spectral phases (J. Bayer et al. 2021; J. Johansson et al. 2021; W. Chen et al. 2024); (iii) some SNe are "standardisable," providing absolute magnifications to break degeneracies of lens modeling (L. Weisenbach et al. 2024); and (iv) after the supernova has faded the lensed host galaxy can be used to constrain the lensing potential without the noise and systematics of overlapping bright point sources (as used for iPTF16geu in, e.g., E. Mörtsell et al. 2020).

While cluster-scale lensed supernovae have already been used for time-delay cosmography (e.g., J. Vega-Ferrero et al. 2018; P. L. Kelly et al. 2023; M. Pascale et al. 2025;

[71] NHFP Einstein Fellow.
[72] CCAPP Fellow.

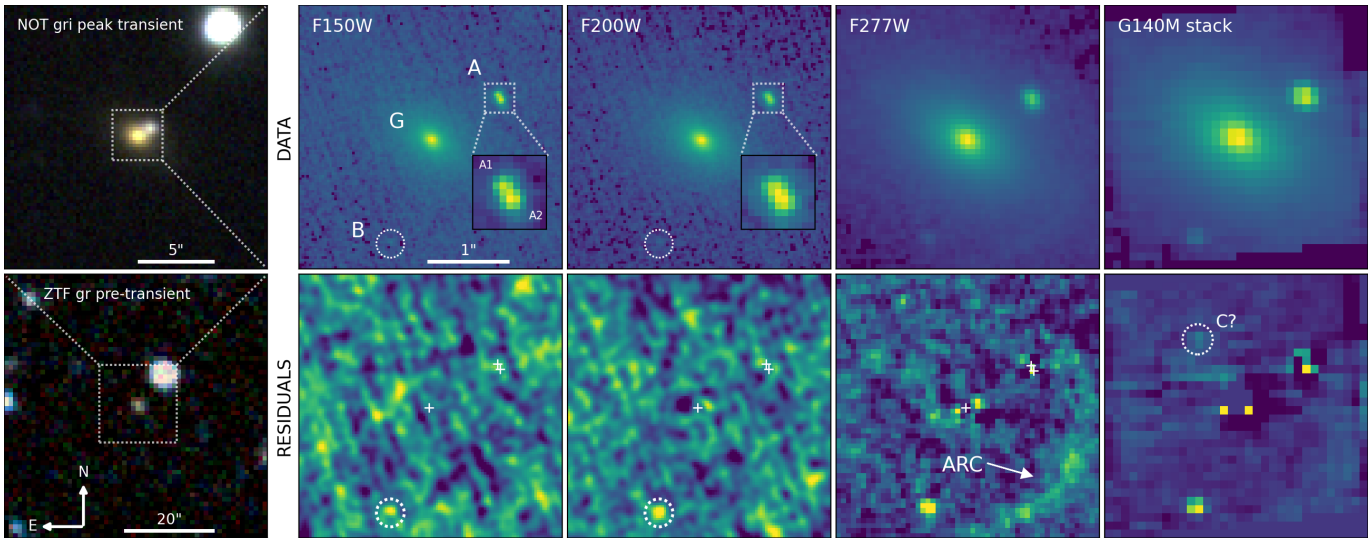

Figure 1. Left: ZTF *gr* image of the field before the transient (bottom) and NOT *gri* image during the peak of the lightcurve (top). Right: NIRCam F150W, F200W, and F277W images, alongside the NIRSpec G140M white light image (top), and subtractions after modeling the lensing galaxy, G, and image A (bottom). Note the inset showing that image A is well modeled as two PSFs separated by $\sim 0\farcs07$. The F277W and G140M residuals show an arc to the south west of the galaxy, as well as a hint of another image, which we label C.

J. D. R. Pierel et al. 2025), the mass models are complex and do not completely use the information of the lensed arcs. Galaxy-scale lensed supernovae offer a promising route to the Hubble constant, thanks to their simple lens mass distributions, though the first examples discovered had time delays too short to offer competitive cosmological constraints (A. Goobar et al. 2017, 2023a). Recently J. Johansson et al. (2025) and S. Taubenberger et al. (2025) reported a lensed Type I superluminous supernova at $z = 2.01$ with a maximum image separation of $4\farcs9$.

In this Letter, we report the discovery of SN 2025mkn at $z = 1.371$, a Type II supernova that is multiply imaged by a foreground galaxy at $z = 0.42$, with lens coordinates of R.A., decl. (J2000) = 16:42:11.47, +55:31:02.45. In Section 2, we outline both ground-based and JWST imaging and spectra, and in Section 3 we present analysis of the source, the lensing galaxy, and present a simple lens model of the system. We discuss the data, model, and implications in Section 4, and conclude in Section 5. Throughout this work, we adopt a flat ΛCDM cosmology with $\Omega_m = 0.3$, $\Omega_\Lambda = 0.7$, and $H_0 = 70\,\mathrm{km\,s^{-1}\,Mpc^{-1}}$. Magnitudes are reported in the AB system.

2. Observations

Previous galaxy-scale lensed supernovae have been discovered through an inferred magnification. This requires a redshift and expected absolute magnitude. Ideally, spectra will provide both the redshift and supernova type (and thus expected intrinsic brightness); however, spectra are costly and rare for these types of events. To expand the search, photometric redshifts of potential host galaxies are used so photometric candidates can also be vetted (D. A. Goldstein & P. E. Nugent 2016). In the case of lensing, even though the lensing galaxy will be incorrectly assumed to be a host, it still provides a lower redshift limit with which to search for overly bright supernovae. Our search for lensed supernovae is based on the cadenced survey by the Zwicky Transient Facility (ZTF; E. C. Bellm et al. 2019; D. A. Duev et al. 2019; M. J. Graham et al. 2019; A. Mahabal et al. 2019; F. J. Masci et al. 2019; M. T. Patterson et al. 2019; R. Dekany et al. 2020).

During our daily automatic crossmatch of new ZTF transients to photometric redshifts, SN 2025mkn—internally named ZTF25aasjeza—was alerted as a transient with an intrinsic magnitude of $M = -22.4 \pm 0.1$ given the nearby photometric redshift of $z = 0.39 \pm 0.02$ (Legacy Survey; R. Zhou et al. 2021). A Dark Energy Spectroscopic Instrument (DESI; DESI Collaboration et al. 2016, 2022; J. Guy et al. 2023; E. F. Schlafly et al. 2023; T. N. Miller et al. 2024; C. Poppett et al. 2024; M. Abdul Karim et al. 2025; A. G. Adame et al. 2025; DESI Collaboration et al. 2026; S. Bailey et al. 2026, in preparation) spectrum of the galaxy confirmed it to be $z = 0.4203 \pm 0.0001$. The spectrum was taken from the internal release "Loa", which will be released as part of DESI DR2 in 2027.[73] The transient was also reported by the Asteroid Terrestrial-impact Last Alert System (ATLAS; J. L. Tonry et al. 2018).

An early classification spectrum of the transient by the Spectroscopic Classification of Astronomical Transients (SCAT) survey (M. A. Tucker et al. 2022; J. Hinkle 2025) showed a nearly featureless blue spectrum. However, upon closer inspection, narrow absorption lines are present at two distinct redshifts, $z = 1.256$ and $z = 1.371$. This provides a new lower limit for the supernova redshift of 1.371, implying a rest-frame UV absolute magnitude $M \sim -25$ mag, which is several magnitudes brighter than the most extreme superluminous supernovae; thus, a lensing magnification is required, which was reported in A. Goobar et al. (2025). This led to the triggering of a JWST program, involving imaging that resolves the multiple lensed images (see Figure 1) and spectroscopy, both of which we present in this section, alongside a ground-based follow-up. We also obtained Karl G. Jansky Very Large Array (VLA; A. R. Thompson et al. 1980; R. A. Perley et al. 2011) observations to investigate the source as a possible Luminous Fast Blue Optical Transient (LFBOT), which yielded a nondetection.

[73] DESI spectrum ID 39633329464544708, available in DESI DR2.

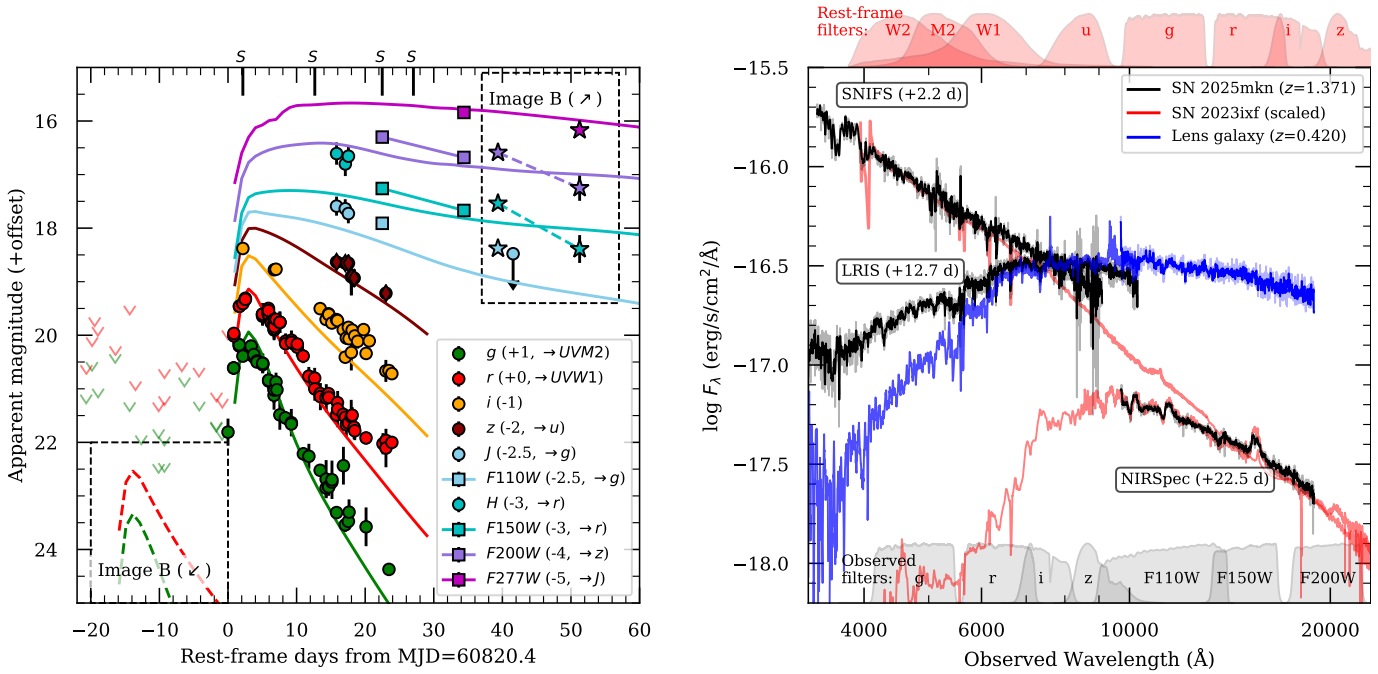

Figure 2. Left panel: compilation of ground-based (circles) and JWST (square symbols) photometric observations of SN 2025mkn (Image A). The solid lines show the lightcurves of SN 2023ixf in matching rest-frame filters or synthetic photometry on spectra indicated in the legend. The star symbols and dashed lines show the photometry for image B (shifted both in time and magnitude, corresponding to a fiducial time delay and differential magnification). The observation dates of the spectra are marked along the top with "S" symbols. Right panel: optical and near-IR spectra (black lines) of SN 2025mkn (Image A). The shaded red lines show SN 2023ixf redshifted and scaled to match SN 2025mkn with magnifications of 250 and 15 (for A and B respectively) at similar phases (reported in rest-frame days). The blue line is a combined Keck/LRIS and JWST/NIRSpec spectrum of the lens galaxy.

The long-wavelength JWST/NIRCam data (Figure 1) clearly resolve both the lensing galaxy and the transient seen north west of the galaxy. They also show a second point source 1.″3 south east of the galaxy. We label the two point sources A and B, respectively, and note that B is approximately 30 times fainter than A. We postulate that B is another image of the transient, and provide supporting evidence in the next section.

2.1. Ground-based Imaging

The ZTF *g*- and *r*-band lightcurves of SN 2025mkn are supplemented by *gri* photometry from both the Spectral Energy Distribution Machine (SEDM; N. Blagorodnova et al. 2018; M. Rigault et al. 2019; Y.-L. Kim et al. 2022) on the Palomar 60-inch telescope and the Alhambra Faint Object Spectrograph and Camera (ALFOSC) on the Nordic Optical Telescope, and *griz* observations with the IO:O camera on the Liverpool Telescope (LT), and *grzJH* imaging with the Fraunhofer Telescope at Wendelstein Observatory (FTW) using the Three Channel Imager (3KK; F. Lang-Bardl et al. 2016).

For the optical griz data we use archival Pan-STARRS (K. C. Chambers et al. 2016) images for subtractions. For 3KK, the optical CCD and near-infrared (NIR) CMOS data were reduced using a custom pipeline (C. A. Gössl & A. Riffeser 2002; M. Busmann et al. 2025). For the astrometric calibration of the images, we used the Gaia EDR3 catalog (Gaia Collaboration 2020; Gaia Collaboration et al. 2021; L. Lindegren et al. 2021). Tools from the AstrOmatic software suite (E. Bertin & S. Arnouts 1996; E. Bertin et al. 2002; E. Bertin 2006) were used for the coaddition of each epoch's individual exposures (as well as for the IR imaging described later). We use the Saccadic Fast Fourier Transform (`SFFT`; L. Hu et al. 2022) algorithm for image subtraction.

For the near-IR *J*- and *H*-band data, we follow the same image subtraction process as for the optical imaging, but calibrate against the 2MASS Catalog (M. F. Skrutskie et al. 2006). For 3KK, we use templates from the United Kingdom Infrared Telescope (UKIRT; S. Dye et al. 2018).

Due to the high decl. of SN 2025mkn, ZTF observations of the field have short seasonal gaps of ∼55 days. In the discovery season, data starting ∼170 days before peak are available in the *g* and *r* bands with a median cadence of ∼2–3 days. In these data, we search for any preceding images, and in the case of a nondetection, place upper limits on the brightness.

We download all epochs of available *g* and *r* imaging from ZTF through the IRSA ZTF application programming interface (API), to build a scene model of the pretransient system, using `lightcurver` (F. Dux 2024) and `STARRED` (K. Michalewicz et al. 2023). After subtracting the best-fit constant model (the lensing galaxy and a nearby star), the residuals are inspected for signs of leading images. No detection is seen in any epoch before image A first appears. 5σ nondetections are shown in Figure 2. The photometric datasets were collated using `fritz` (S. van der Walt et al. 2019; M. W. Coughlin et al. 2023).

In Figure 2 we show all of the available photometry for this system, with the lightcurves of the nearby Type II supernova, SN 2023ixf, overlaid, with discussion on the nature of the source in Section 3.1.

2.2. Ground-based Spectra

On 2025 May 30, a classification spectrum was taken with the SuperNova Integral Field Spectrograph (SNIFS; B. Lantz et al. 2004) on the University of Hawaii 2.2 m telescop SCAT (M. A. Tucker et al. 2022). SNIFS covers the full optical range

Table 1
Synthetic Photometry from NIRSpec (MJD = 60873.7) and Photometry from NIRCam Imaging (MJD = 60901.9)

Object	NIRSpec [MJD = 60874]			NIRCam [MJD = 60902]			Astrometry + Lens model				
	F110W	F150W	F200W	F150W	F200W	F277W	$-\Delta$R.A.cos δ (arcsec)	ΔDecl. (arcsec)	κ	γ	μ
A	$20.41^{+0.05}_{-0.05}$	$20.26^{+0.05}_{-0.05}$	$20.30^{+0.05}_{-0.05}$	$20.67^{+0.01}_{-0.01}$	$20.68^{+0.01}_{-0.01}$	$20.84^{+0.01}_{-0.01}$	...	...	...	...	...
A1	...	...	...	$21.33^{+0.02}_{-0.02}$	$21.33^{+0.03}_{-0.03}$	...	$0.843^{+0.003}_{-0.003}$	$0.474^{+0.003}_{-0.003}$	0.482	0.508	101
A2	...	...	...	$21.53^{+0.02}_{-0.02}$	$21.54^{+0.03}_{-0.03}$	...	$0.809^{+0.003}_{-0.003}$	$0.540^{+0.003}_{-0.003}$	0.492	0.518	−97
B	$24.28^{+0.05}_{-0.05}$	$23.94^{+0.05}_{-0.05}$	$23.99^{+0.05}_{-0.05}$	$24.79^{+0.26}_{-0.18}$	$24.65^{+0.24}_{-0.20}$	$24.57^{+0.09}_{-0.07}$	$-0.49^{+0.01}_{-0.01}$	$-1.24^{+0.01}_{-0.01}$	0.332	0.346	3.1
G	$18.53^{+0.05}_{-0.05}$	$18.12^{+0.05}_{-0.05}$	$17.90^{+0.05}_{-0.05}$	$18.16^{+0.01}_{-0.01}$	$17.95^{+0.01}_{-0.01}$	$18.00^{+0.01}_{-0.01}$	$0.000^{+0.003}_{-0.003}$	$0.000^{+0.003}_{-0.003}$	...	...	...
A/B flux ratio	∼35	∼30	∼30	48^{+13}_{-9}	39^{+6}_{-5}	32^{+3}_{-2}	68				

Note. Uncertainties are based on the 16th and 84th percentile intervals for NIRCam and we estimate 0.05 for NIRSpec based on agreement of the galaxy magnitude with NIRCam. The galaxy photometry is based on a 1.″0-radius aperture. We also present F200W image astrometry with a fiducial lens model (including convergence, κ, shear γ, and image magnification μ), for which a fourth image is also predicted, at (−0.″55, 0.″82), with $\kappa = 0.632$, $\gamma = 0.606$, and $\mu = -4.3$. The F110W and F200W synthetic magnitudes are based only on the wavelength range overlapping with the NIRSpec Spectrum.

with both a blue (320—560 nm) and a red (520—1000 nm) channel. The SNIFS spectrum was taken in good conditions, with a seeing of ≈0.″8, and had an exposure time of 1800 s. The data were reduced with the custom SCAT reduction pipeline, which incorporates wavelength-dependent tracing across each channel and aperture extraction from the reconstructed data cubes (see M. A. Tucker et al. 2022, for more details).

SN 2025mkn was later observed with the Low Resolution Imaging Spectrometer (LRIS) on the 10m-class telescope Keck I on the nights of 2025 June 24, July 25, and 28, with a 1.″0 wide slit using the B400/3400 grism and R400/8500 grating at a parallactic angle. Two exposures of 600 s were taken, and spectra were reduced and extracted using `LPipe` (D. A. Perley 2019).

2.3. JWST NIRCam

JWST/NIRCam imaging (program 3468, A. Goobar et al. 2023b) was taken in simultaneous short- (SW) and long-wavelength (LW) mode on module B with the FULL subarray, using RAPID readout (two groups per integration; one integration per exposure); the SW channel used F150W and F200W, each paired with F277W in LW. We applied an intramodule `SMALL-GRID-DITHER` (four dithers with sub-pixel steps), obtaining four integrations of 21.5 s each, for a total of 86 s in each of the SW filters, and 172 s in the LW filter. We note that the pixel scales for the SW and LW images are 0.″0312 and 0.″0629 pix^{-1}, respectively. The standard pipeline data showed clear 1/f (flicker) noise (H. Bushouse et al. 2023), evident as horizontal banding in the SW images, so the pipeline was rerun with `clean_flicker_noise` turned on in stage 1, and the `skymatch` process in stage 3 (B. J. Rauscher 2024). The data for the system are shown in each filter in the top row of Figure 1.

2.3.1. Light Modeling

As previously mentioned, the F277W data show the bright transient, A, as well as a fainter point source, B, south east of the lens, which we postulate as another image of the source. We also note that A is elongated in the tangential direction, and appears to be consistent with two point spread functions (PSFs) in the F150W and F200W data. We therefore consider these two images–A1 and A2, as labeled in Figure 1–for the purposes of fitting. To determine galaxy profile parameters and point-source positions, we fit three point sources and two concentric Sérsic profiles, convolved by the same point-source model. We use the `STPSF DET_DIST` extension as our PSF model (M. D. Perrin et al. 2014); although this product is formally intended to match detector-coordinate images (e.g., individual rate exposures), we use it here as an approximation for the drizzled PSF. Given the low signal-to-noise of our data, we expect this PSF estimate to be robust for our current analysis. The galaxy- and A-subtracted residuals (after Gaussian smoothing with widths of 2, 2, and 1 pixels respectively) are shown in the bottom row of Figure 1.

While image B is immediately obvious in the F277W data and the NIRSpec white light image, it is also detected at 5.1σ and 5.3σ significance in the F150W and F200W data respectively, even when allowing its position to vary. We report the photometry and astrometry with their 16th and 84th percentile intervals in Table 1. We also note the presence of an arc-like structure in the south west of the system only seen in the F277W filter of the imaging data, which we postulate to be the lensed host galaxy of the source supernova.

2.4. JWST NIRSPEC IFU

Through program 3468 (A. Goobar et al. 2023b), JWST/NIRSpec integral-field spectroscopy was obtained using the G140M grating with the F100LP filter in Intergral Field Unit (IFU) mode, providing observer-frame spectral coverage from $\lambda \simeq 0.97$ to 1.89 μm (R ∼1000). The data were taken in the `NRS_FULL_IFU` aperture as part of a `4-POINT-DITHER` pattern (a box of ∼0.″4 on a side), in NRSRAPID readout with $N_{\rm INT} = 7$ integrations and $N_{\rm GROUP} = 12$ groups per integration, resulting in an effective exposure time of $t_{\rm exp} = 3600$ s. The data were reduced with the standard JWST NIRSpec pipeline (H. Bushouse et al. 2023), and the spatial pixel scale is 0.″10 spaxel^{-1}.

In many slices, artefacts with diamond-shaped patterns were present—with the same shape as the dither pattern—and were masked by hand. For each slice of the combined product with north up, background striping oriented along one axis of the instrument frame is seen. Therefore, in the following modeling process, we fit a varying background perpendicular to this direction, such that at each pixel step along this perpendicular direction, a degree of freedom for a constant background is allowed.

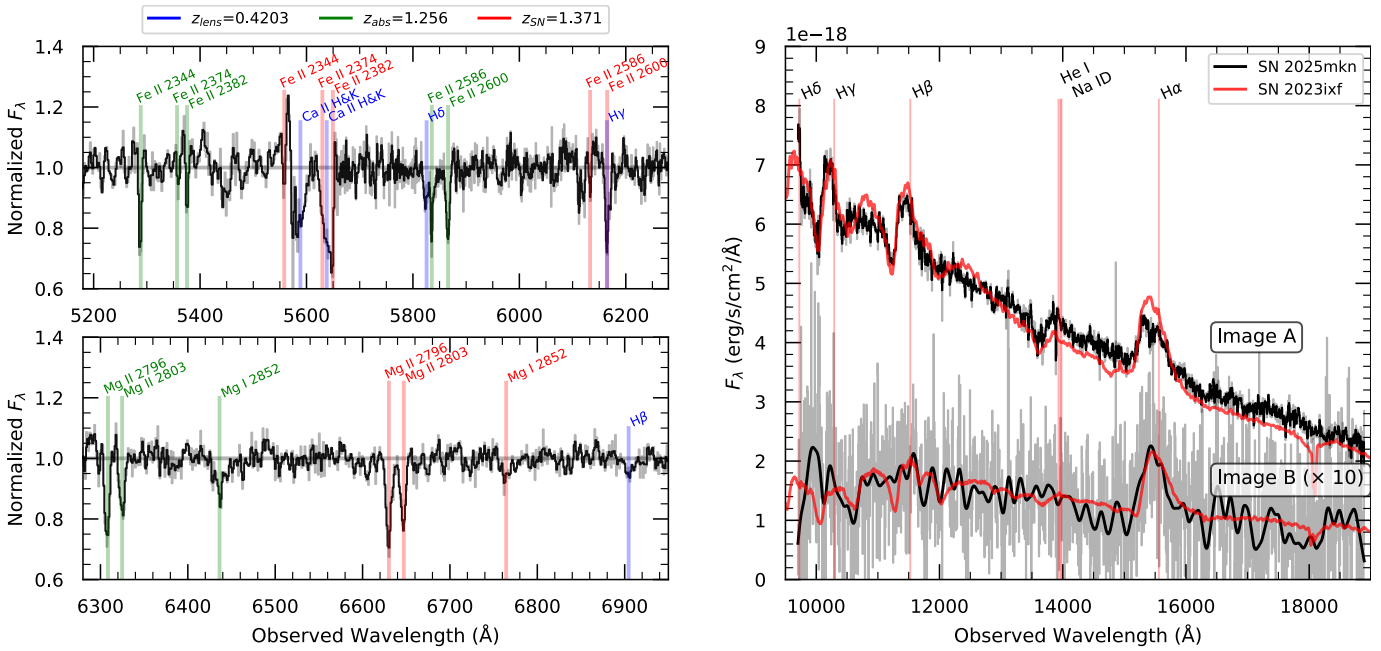

Figure 3. Left panel: selection of narrow absorption features seen in the LRIS spectrum of SN 2025mkn (here showing the continuum normalized Keck/LRIS spectrum from 2025 June 24). The spectrum shows absorption features from the lens galaxy at $z = 0.420$ (blue lines), as well as from systems at $z = 1.256$ (green) and $z = 1.371$ (red lines). Right panel: JWST/NIRSpec spectra of SN 2025mkn Images A and B (black lines). The red lines show SN 2023ixf, redshifted to $z = 1.371$ and scaled to match SN 2025mkn.

In the white light image of the cube (see Figure 1), image B is clearly detected. Image A is unresolved in the NIRSpec image so we extract it with a single PSF, and include another PSF for image B—as well as a Sérsic profile convolved by that same PSF for the lensing galaxy. The PSF is generated using the `STPSF` package (M. D. Perrin et al. 2014). We use the relative positions as measured from the NIRCAM imaging, only fitting for the galaxy position, so our model at each slice contains two positional degrees of freedom, five for the Sérsic profile, and ∼40 for the varying background. The signal of image B is below the noise in most slices, so we repeat the fit by stacking slices in bins of 10 to extract our final spectrum of B. The 2D stacked data (white light) and residuals are shown in Figure 1, and we note the presence of the arc, which is also seen in the F277W NIRCam data, as well as a possible extra source, which we label as C. The 1D spectrum of A is shown in Figure 2, and the spectra of A and B are compared in more detailed in Figure 3.

The spectrum of B shows a peak at the wavelength of Hα expected at $z \sim 1.37$, which now firmly establishes its nature as another image of the source. We therefore also expect that it is fading between the NIRSpec and NIRCam observations (which are separated by 28 days), so we perform synthetic photometry on the NIRSpec 1D spectra of both A and B and present the values in Table 1. We note that the extraction is reliable as we recover the same value for the F150W magnitude of the lensing galaxy in a 1.″0 circular aperture within 0.05 mag. We take this error as an estimated systematic error on our synthetic photometry. We indeed do see that images A and B fade between the observations, and we discuss this further in Section 4.

2.5. VLA Observations

We obtained VLA data of SN 2025mkn under Director's Discretionary Time program VLA/25B-366 (PI: A.Y.Q. Ho). The observation started at 2025 September 2 23:29 UT and lasted 2.5 hr at midfrequencies of 10 GHz (*X*-band, 4 GHz bandwidth) and 15 GHz (Ku-band, 6 GHz bandwidth). We calibrated the data using the automated pipeline in Common Astronomy Software Applications package version 6.5.4–9 (CASA; CASA Team et al. 2022) and imaged using standard techniques. We use the `pwkit/imtool` program (P. K. G. Williams et al. 2017) to measure the flux density and image rms. The foreground lensing galaxy is radio bright, and has a 10 GHz flux density of 205 ± 60 μJy and a 15 GHz flux density of 128 ± 30 μJy. There is no apparent emission at the location of the SN 2025mkn images, and the rms is measured at $\lesssim$4 μJy at 10 GHz and $\lesssim$5 μJy at 15 GHz.

3. Analysis

3.1. Spectra and Lightcurves

The early SNIFS spectrum exhibits a steep blue continuum with an inferred blackbody temperature of ∼27,000 K and an absence of obvious broad supernova features.

Superimposed on the two first spectra are multiple narrow absorption lines. As shown in the left panel of Figure 3, we identify prominent Fe II lines and the Mg II $\lambda\lambda$2796, 2803 doublet at two distinct redshifts, $z_1 = 1.256 \pm 0.001$ and $z_2 = 1.371 \pm 0.001$. Additional absorption features at $z_{\rm lens} = 0.420$ correspond to the foreground lensing galaxy.

The higher redshift $z_2 = 1.371$ is adopted as the SN redshift, based on the broad hydrogen features in the JWST/NIRSpec spectrum of image A. At a rest-frame phase of +22.5 days, the spectrum displays broad Hα, Hβ, and Hδ emission features, unambiguously identifying SN 2025mkn as a Type II supernova. The NIRSpec spectrum of image B likewise exhibits broad Hα emission at the same redshift, firmly establishing it as a second lensed image of the same explosion. The presence of fading between the NIRSpec and NIRCam epochs further confirms the transient nature of image B.

The photometric evolution of image A is shown in Figure 2, combining ground-based optical and near-infrared data with resolved JWST photometry. The lightcurves exhibit a close resemblance in shape to those of Type II supernovae, the nearby IIP/IIL SN 2023ixf in particular (E. A. Zimmerman et al. 2024), when compared in matched rest-frame filters. Motivated by this striking similarity, we use SN 2023ixf as a local analog to estimate the magnification of SN 2025mkn.

Under the assumption that SN 2025mkn follows the intrinsic luminosity evolution of SN 2023ixf, the observed peak brightness of image A implies a magnification of $\Delta m_{\rm A} \sim 6$ mag, corresponding to $\mu_{\rm A} \sim 250$. Independent estimates from spectral scaling yield consistent results: matching the flux-calibrated spectra of images A and B to SN 2023ixf at similar phases implies magnifications of $\mu_{\rm A} \sim 250$ and $\mu_{\rm B} \sim 15$, respectively. It should be noted that SNe II show significant peak-brightness scatter ($\sigma \sim$ 1 mag), limiting the precision of magnification estimates based on their luminosity. Hence, next we estimate the magnification independent of the assumption that SN 2023ixf and SN 2025mkn are exact analogs in Section 3.3 through lens modeling.

The spectral comparison further reveals that image B appears at a later phase than image A, consistent with a significant time delay between the two images. Although the leading image was not detected in archival ZTF data (see inset dashed lines in Figure 2), the relative spectral phases provide an independent handle on the time delay, an approach that will be explored in detail in a forthcoming companion paper (J. Johansson et al. 2026, in preparation).

3.2. Lens Galaxy

Estimating the total mass and properties of the lensing galaxy is an important step in prioritizing follow-up of lensed supernova candidates. In particular, the mass of the lensing galaxy provides an estimate of the image separation of potential multiple images.

We derive the stellar mass of the system using Pan-STARRS *grizy* (K. C. Chambers et al. 2016; H. A. Flewelling et al. 2020; E. A. Magnier et al. 2020), 2MASS JHK_S (M. F. Skrutskie et al. 2006), and WISE W1 − W4 (E. L. Wright et al. 2010) photometry, taken from `blast` (D. O. Jones et al. 2024). The measured fluxes before extinction correction are (11.57 ± 0.71, 48.56 ± 1.01, 83.84 ± 1.03, 115.61 ± 2.51, 133.13 ± 5.32, 191.52 ± 86.72, 487.82 ± 131.79, 477.98 ± 152.5, 263.7 ± 11.76, 184.48 ± 13.24, 31.84 ± 29.59, -103.5 ± 258.64) μJy in (g, r, i, z, y, J, H, K_S, W1, W2, W3, W4). We apply a Milky Way reddening correction using the K. D. Gordon et al. (2023) UV–mid-infrared extinction law, with $E(B-V) = 0.012$ mag from the E. F. Schlafly & D. P. Finkbeiner (2011) dust map, with $R_V = 3.1$. We perform a Bayesian spectral energy distribution (SED) fit using the `prospector` modeling framework (B. D. Johnson et al. 2021) with a stellar population synthesis (SPS) model based on the Flexible Stellar Population Synthesis code (FSPS; C. Conroy et al. 2009, 2010; C. Conroy & J. E. Gunn 2010), and a parameterization based on Prospector-α (J. Leja et al. 2017, 2019b). We use a G. Chabrier (2003) stellar initial mass function, and a seven-bin star formation history with bins logarithmically spaced in lookback time (J. Leja et al. 2019a, 2019b). Nebular emission is included based on the `cloudy` (G. J. Ferland et al. 2013) model grid from N. Byler et al. (2017). We carry out posterior sampling using the `dynesty` (J. S. Speagle 2020) nested sampler, with a sampling strategy based on J. Skilling (2004, 2006), F. Feroz et al. (2009), and E. Higson et al. (2019). We estimate a lens mass of $\log_{10}(M/M_\odot) \approx 11.4 \pm 0.1$, which provides an estimated Einstein radius of $(1.04 \pm 0.12)''$ (ignoring aperture corrections and the presence of dark matter).

We can independently determine the Einstein radius using the velocity dispersion from the DESI spectrum: 281 ± 50 km s^{-1}. Given the redshifts of the lens and source, and under the assumption of an isothermal mass profile, we constrain $\theta_E = (1.38 \pm 0.45)''$, in agreement with the estimate from the stellar mass estimate.

Multiple images in strongly lensed systems are typically separated by twice the Einstein radius—therefore, at least $2''$ in the case of SN 2025mkn. Given that image A lies only $\sim 0\farcs8$ from the galaxy, another more distant image is expected opposite the lens. Coupled with the magnification argument from the source intrinsic magnitude, our Einstein radius estimate convincingly demonstrated a case of strong lensing, which was borne out by the discovery of image B in the JWST datasets.

3.3. Lens Model

Before we discuss the nature of the system based on the above analysis, we will provide a lens model based on the astrometry of the SW NIRCam imaging.

As previously discussed, image B is a counterimage of the supernova due to the Einstein radius estimates, spectroscopic redshift from NIRSpec, and its transient nature (fading between datasets). We also take A1 and A2 to be separate images of the transient since they are each consistent with point sources, and have the same F200W–F150W color based on the resolved JWST NIRCam imaging.

To elucidate the nature of the system, we fit a simple lens model of a singular isothermal ellipsoid with external shear to recover these three images using `lenstronomy` (S. Birrer & A. Amara 2018; S. Birrer et al. 2021), but do not place any constraints on the required flux ratios. We only have 6° of freedom (from three image positions), so we fix the lens mass to that measured from the light, i.e., the centroid and flattening parameters–150° north of east with an axis ratio of 0.634–and only fit for five parameters: the Einstein radius, external shear strength and position angle, and a source position.

We show our best-fit lensing model in Figure 4, demonstrating the recovery of the image positions and large magnifications of images A1 and A2. The reduced χ^2 is 2.1. We note that in all models a fourth image is predicted, which we label C, and note that the time delays are similar to those of images A1 and A2, and thus should be closer to peak than image B. Even ignoring this phase, the lens model predicts it to be brighter than image B; however, it is not seen in any of the imaging data. Its predicted position is compatible with a potential detection in the NIRSpec white light residuals (see Figure 1), as described in Section 2.4. Values for the convergence, shear, and magnifications are provided in Table 1. The total magnification of our best-fit model is $\sim$200, and the predicted flux ratio of A (A1+A2) to B is $\sim$65. While this is at odds with the observed upper limit of 30 from the NIRSpec flux ratio, we find that much lower total magnifications are possible when the lens mass is allowed to deviate from the light. We discuss alternative explanations for this in Section 4, while keeping the lens mass and light aligned.

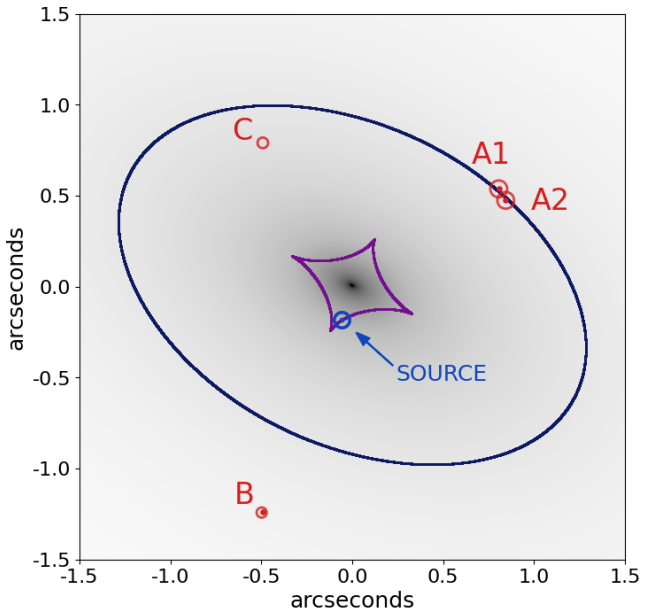

Figure 4. Best-fit elliptical power law with external shear mass model for SN 2025mkn, with predicted image positions as open red circles. The model recovers the observed positions (red dots) of A1, A2, and B, but also predicts a fourth image, C. The source lies close to the astroid caustic (purple), and the high-magnification images of A straddle the critical curve (dark blue).

The model Einstein radius is $\sim 1\farcs12$, and the external shear strength is 0.03 at 128° north of east. This small external shear gives confidence to our assumption that the lens mass follows the light. While our model predicts a time delay of weeks between images A and B, we do not report an exact value here for the sake of blinding any potential time-delay measurements from spectral phase matching of the spectra of images A and B. However, we do note that the predicted time delay between images A1 and A2 is approximately 1 minute—not measurable.

More detailed lens models, which include the information in the lensed host galaxy arc, will be presented in an upcoming paper alongside the spectral time-delay measurements.

4. Discussion

The magnification estimate of $\times 250$, based on the assumption of a SN 2023ixf analog, is in agreement with the light-mass-aligned lens models, which can predict total magnifications up to 300. However, there are two problems when confronting the lens model to the data: (i) image C is predicted to be brighter than B but is not seen in the imaging data (an upper limit from the F277W data for C is around 0.25 times the brightness of B, or 1.5 magnitudes fainter); and (ii) the flux ratio of A (A1+A2 combined) to B is measured to be around 25 accounting for the time delay, but predicted to be ~ 65 from the lens model. These discrepancies can be explained by a different lens model in which the lens mass is allowed to deviate from the light. Such models (while underconstrained with just the three image positions) can reproduce the observed A to B ratio of 25–30, though C is still expected at a similar brightness to B.

We can resolve flux ratio problems in either case by invoking microlensing of a combination of images B and C. Images A1 and A2 are unlikely to be significantly affected by microlensing due to their similar flux ratio—as predicted by the model. From the NIRSpec white light image we estimate that the brightness of the potential detection of image C is around 25% the brightness of B, consistent with the lack of detection in the NIRCam imaging. We therefore require the B/C brightness to be boosted by a factor of ~ 4. While reducing the flux of image C can explain this, also boosting the flux of image B can help explain the A/B ratio in the mass-light-aligned models.

We generate microlensing maps given the best-fit κ-γ values from our model (J. Jiménez-Vicente & E. Mediavilla 2022), assuming a smooth matter fraction of 0.5 (typical for images of similar lenses) and stellar masses of 0.2 $M_{\odot}$ (such that the Einstein radii match the photospheric scale of a type II supernova 40–50 days post-explosion). Image C is demagnified by 0.8 mag or more in 49% of cases (demagnification is common for saddle points; P. L. Schechter & J. Wambsganss 2002), while B is only magnified by 1 mag or more in 6% of cases. By drawing random realizations of the microlensing in images B and C, and comparing the relative probability of these cases to the most probable case, we find that requiring the above (de)magnifications is more probable than 20% of such realizations.

This shows that the observed flux ratios can be satisfactorily explained with microlensing, though the exact reliance on this requires a better-constrained mass model, which will be the focus of future investigations using the information of the extended host arc, and possibly by extracting a position constraint from image C.

5. Conclusions

We have presented the discovery of SN 2025mkn as a gravitationally lensed Type II supernova, with a magnification of $\times 100$ or larger, potentially reaching ~ 250 if interpreted as a near-perfect analog of SN 2023ixf. This system is unique not only as the most magnified supernova yet discovered, but as the first single galaxy lensed supernova with a time delay of weeks. These extreme magnification events are expected in magnitude-limited surveys, such as the previous galaxy-scale spectroscopic discoveries (A. Goobar et al. 2017, 2023a); however, in this case the flux ratio between images is extreme, and might not be expected in mock catalogs that require several, or leading, images to be brighter than a certain threshold (e.g., M. Oguri & P. J. Marshall 2010). The striking photometric and spectroscopic resemblance with SN 2023ixf, one of the best studied Type II supernovae in the local Universe, from the rest-frame far-UV to the near-IR, emphasizes the power of lensing magnification to constrain evolutionary effects in stellar explosions over 9 Gyrs. Such detailed comparisons for unlensed supernovae are at the limits of observing capabilities of existing telescopes, as demonstrated by the study of a lensed Type II supernova at $z = 5$ (D. A. Coulter et al. 2026). Triggering follow-up for such systems as soon as possible is key to maximizing their scientific use. Robust photometric or spectroscopic redshifts of early type galaxies, and estimates of Einstein radii from stellar mass estimates or velocity dispersions help to prioritize the limited spectroscopic follow-up.

One major difficulty of turning this system into a cosmographic probe is the leading image being too faint to obtain a resolved lightcurve. Despite only triggering follow-up long after it faded, spectroscopic phase retrieval offers a way to measure the time delay, especially in the case of an archival local analog with well-sampled UV spectra. In an upcoming

paper we will present detailed lens models including modeling of the extended arc, alongside time-delay measurements from the resolved JWST NIRSpec spectra, and any associated cosmological constraints.

Acknowledgments

We thank the Space Telescope Science Institute (STScI) support staff for their assistance with the planning and execution of the JWST observations, and for helpful guidance throughout the observing program.

Based on observations obtained with the Samuel Oschin Telescope 48 inch and the 60-inch Telescope at the Palomar Observatory as part of the Zwicky Transient Facility project. ZTF is supported by the National Science Foundation under Award 2407588 and a partnership including Caltech, USA; Caltech/IPAC, USA; University of Maryland, USA; University of California, Berkeley, USA; University of Wisconsin at Milwaukee, USA; Cornell University, USA; Drexel University, USA; University of North Carolina at Chapel Hill, USA; Institute of Science and Technology, Austria; National Central University, Taiwan; and OKC, University of Stockholm, Sweden. Operations are conducted by Caltech's Optical Observatory (COO), Caltech/IPAC, and the University of Washington at Seattle, USA.

SED Machine is based upon work supported by the National Science Foundation under grant 1106171.

The Liverpool Telescope is operated on the island of La Palma by Liverpool John Moores University in the Spanish Observatorio del Roque de los Muchachos of the Instituto de Astrofisica de Canarias with financial support from the UK Science and Technology Facilities Council.

Based on observations made with the Nordic Optical Telescope, owned in collaboration by the University of Turku and Aarhus University, and operated jointly by Aarhus University, the University of Turku and the University of Oslo, representing Denmark, Finland, and Norway, the University of Iceland, and Stockholm University at the Observatorio del Roque de los Muchachos, La Palma, Spain, of the Instituto de Astrofisica de Canarias. The NOT data were obtained under program ID P70-501.

Some of the data presented herein were obtained at the W. M. Keck Observatory, which is operated as a scientific partnership among the California Institute of Technology, the University of California, and NASA. The Observatory was made possible by the generous financial support of the W. M. Keck Foundation. The authors wish to recognize and acknowledge the very significant cultural role and reverence that the summit of Maunakea has always had within the indigenous Hawaiian community. We are most fortunate to have the opportunity to conduct observations from this mountain.

This material is based upon work supported by the U.S. Department of Energy (DOE), Office of Science, Office of High-Energy Physics, under Contract No. DE–AC02–05CH11231, and by the National Energy Research Scientific Computing Center, a DOE Office of Science User Facility under the same contract. Additional support for DESI was provided by the U.S. National Science Foundation (NSF), Division of Astronomical Sciences under Contract No. AST-0950945 to the NSF's National Optical-Infrared Astronomy Research Laboratory; the Science and Technology Facilities Council of the United Kingdom; the Gordon and Betty Moore Foundation; the Heising-Simons Foundation; the French Alternative Energies and Atomic Energy Commission (CEA); the National Council of Humanities, Science and Technology of Mexico (CONAHCYT); the Ministry of Science, Innovation and Universities of Spain (MICIU/AEI/10.13039/501100011033); and by the DESI Member Institutions: https://www.desi.lbl.gov/collaborating-institutions. Any opinions, findings, and conclusions or recommendations expressed in this material are those of the author(s) and do not necessarily reflect the views of the U. S. National Science Foundation, the U. S. Department of Energy, or any of the listed funding agencies.

The Photometric Redshifts for the Legacy Surveys (PRLS) catalog used in this Letter was produced thanks to funding from the U.S. Department of Energy Office of Science, Office of High Energy Physics via grant DE-SC0007914.

The authors are honored to be permitted to conduct scientific research on I'oligam Du'ag (Kitt Peak), a mountain with particular significance to the Tohono O'odham Nation.

C.L. acknowledges funding from the European Union's Horizon Europe research and innovation program under the Marie Sklodovska-Curie grant agreement No. 101105725. A. G. acknowledges financial support from the research project grant "Understanding the Dynamic Universe" funded by the Knut and Alice Wallenberg under Dnr KAW 2018.0067, *Vetenskapsradet*, the Swedish Research Council through grants project Dnr 2020-03444, the G.R.E.A.T research environment, Dnr 2016-06012, and the Swedish National Space Agency, Dnr 2023-00226. I.A. is supported by the National Science Foundation award AST 2505775, NASA grant 24-ADAP24-0159, Scialog award SA-LSST-2024-102a, and the Discovery Alliance Catalyst Fellowship Mentors award 2025-62192-CM-19. S.D. acknowledges support from UK Research and Innovation (UKRI) under the UK government's Horizon Europe funding Guarantee EP/Z000475/1. E. M. acknowledges support from the Swedish Research Council under Dnr VR 2024-03927. I.A. is supported by the National Science Foundation award AST 2505775, NASA grant 24-ADAP24-0159, Scialog award SA-LSST-2024-102a, and the Discovery Alliance Catalyst Fellowship Mentors award 2025-62192-CM-19. M.W.C. acknowledges support from the National Science Foundation with grant numbers PHY-2117997, PHY-2308862 and PHY-2409481. M.B. is supported by a Wübben Stiftung Wissenschaft Student Grant. Funded in part by the Deutsche Forschungsgemeinschaft (DFG, German Research Foundation) under Germany's Excellence Strategy–EXC-2094/2–390783311. This Letter contains data obtained at the Wendelstein Observatory of the Ludwig-Maximilians University Munich. We thank Christoph Ries, Michael Schmid, and Silona Wilke for carrying out the observations. J.T.H. acknowledges support from NASA through the NASA Hubble Fellowship grant HST-HF2-51577.001-A, awarded by STScI. STScI is operated by the Association of Universities for Research in Astronomy, Incorporated, under NASA contract NAS5-26555. TER-T is supported by the Swedish Research Council grant #2022-04805. S.T. has been supported by funding from the European Research Council (ERC) under the European Union's Horizon 2020 research and innovation programs (grant agreement no. 101018897 CosmicExplorer), and from the research project grant "Understanding the Dynamic Universe" funded by the Knut and Alice Wallenberg Foundation under Dnr KAW 2018.0067. M.A.T. is supported by Program number HST-GO-17429.001-A with

funding provided through a grant from the STScI under NASA contract NAS5-26555.

Data Availability

Some of the data presented in this Letter were obtained from the Mikulski Archive for Space Telescopes (MAST) at the Space Telescope Science Institute. The specific observations analyzed can be accessed via doi:10.17909/bs3w-2z02.

ORCID iDs

Cameron Lemon https://orcid.org/0000-0003-2456-9317
Ariel Goobar https://orcid.org/0000-0002-4163-4996
Joel Johansson https://orcid.org/0000-0001-5975-290X
Edvard Mörtsell https://orcid.org/0000-0002-8380-6143
Steve Schulze https://orcid.org/0000-0001-6797-1889
Igor Andreoni https://orcid.org/0000-0002-8977-1498
Aleksandra Bochenek https://orcid.org/0009-0008-2714-2507
Seán J. Brennan https://orcid.org/0000-0003-1325-6235
Malte Busmann https://orcid.org/0009-0001-0574-2332
Michael Coughlin https://orcid.org/0000-0002-8262-2924
Kaustav K. Das https://orcid.org/0000-0001-8372-997X
Suhail Dhawan https://orcid.org/0000-0002-2376-6979
Christoffer Fremling https://orcid.org/0000-0002-4223-103X
Anjasha Gangopadhyay https://orcid.org/0000-0002-3884-5637
Daniel Gruen https://orcid.org/0000-0003-3270-7644
Xander J. Hall https://orcid.org/0000-0002-9364-5419
Anna Y. Q. Ho https://orcid.org/0000-0002-9017-3567
Mansi M. Kasliwal https://orcid.org/0000-0002-5619-4938
Daniel A. Perley https://orcid.org/0000-0001-8472-1996
Mickael Rigault https://orcid.org/0000-0002-8121-2560
Genevieve Schroeder https://orcid.org/0000-0001-9915-8147
Mathew Smith https://orcid.org/0000-0002-3321-1432
Jesper Sollerman https://orcid.org/0000-0003-1546-6615
Jean J. Somalwar https://orcid.org/0000-0001-8426-5732
Robert Stein https://orcid.org/0000-0003-2434-0387
Stephen Thorp https://orcid.org/0009-0005-6323-0457
Alice Townsend https://orcid.org/0000-0001-6343-3362
Jacob L. Wise https://orcid.org/0000-0003-0733-2916
Lin Yan https://orcid.org/0000-0003-1710-9339
Nikki Arendse https://orcid.org/0000-0001-5409-6480
Eric C. Bellm https://orcid.org/0000-0001-8018-5348
Tracy X. Chen https://orcid.org/0000-0001-9152-6224
Andrew Drake https://orcid.org/0000-0003-0228-6594
Frank J. Masci https://orcid.org/0000-0002-8532-9395
Josiah Purdum https://orcid.org/0000-0003-1227-3738
Roger Smith https://orcid.org/0000-0001-7062-9726
Jason T. Hinkle https://orcid.org/0000-0001-9668-2920
T. Emil Rivera-Thorsen https://orcid.org/0000-0002-9204-3256
Benjamin J. Shappee https://orcid.org/0000-0003-4631-1149
Michael A. Tucker https://orcid.org/0000-0002-2471-8442
Jessica Aguilar https://orcid.org/0000-0003-0822-452X
Steven Ahlen https://orcid.org/0000-0001-6098-7247
Davide Bianchi https://orcid.org/0000-0001-9712-0006
David Brooks https://orcid.org/0000-0002-8458-5047
Axel de la Macorra https://orcid.org/0000-0002-1769-1640
John Della Costa https://orcid.org/0000-0003-0928-2000
Arjun Dey https://orcid.org/0000-0002-4928-4003
Peter Doel https://orcid.org/0000-0002-6397-4457
Andreu Font-Ribera https://orcid.org/0000-0002-3033-7312
Jaime E. Forero-Romero https://orcid.org/0000-0002-2890-3725
Enrique Gaztañaga https://orcid.org/0000-0001-9632-0815
Satya Gontcho A. Gontcho https://orcid.org/0000-0003-3142-233X
Gaston Gutierrez https://orcid.org/0000-0003-0825-0517
Dragan Huterer https://orcid.org/0000-0001-6558-0112
Mustapha Ishak https://orcid.org/0000-0002-6024-466X
Jorge Jimenez https://orcid.org/0000-0001-8528-3473
Dick Joyce https://orcid.org/0000-0003-0201-5241
Stephanie Juneau https://orcid.org/0000-0002-0000-2394
Robert Kehoe https://orcid.org/0000-0002-7101-697X
Alex G. Kim https://orcid.org/0000-0001-6315-8743
David Kirkby https://orcid.org/0000-0002-8828-5463
Theodore Kisner https://orcid.org/0000-0003-3510-7134
Anthony Kremin https://orcid.org/0000-0001-6356-7424
Martin Landriau https://orcid.org/0000-0003-1838-8528
Laurent Le Guillou https://orcid.org/0000-0001-7178-8868
Michael E. Levi https://orcid.org/0000-0003-1887-1018
Aaron Meisner https://orcid.org/0000-0002-1125-7384
Ramon Miquel https://orcid.org/0000-0002-6610-4836
John Moustakas https://orcid.org/0000-0002-2733-4559
Seshadri Nadathur https://orcid.org/0000-0001-9070-3102
Brendan O'Connor https://orcid.org/0000-0002-9700-0036
Antonella Palmese https://orcid.org/0000-0002-6011-0530
Will J. Percival https://orcid.org/0000-0002-0644-5727
Ignasi Pérez-Ràfols https://orcid.org/0000-0001-6979-0125
Claire Poppett https://orcid.org/0000-0003-0512-5489
Eusebio Sanchez https://orcid.org/0000-0002-9646-8198
David Schlegel https://orcid.org/0000-0002-5042-5088
Arman Shafieloo https://orcid.org/0000-0001-6815-0337
Joseph Silber https://orcid.org/0000-0002-3461-0320
David Sprayberry https://orcid.org/0000-0001-7583-6441
Gregory Tarlé https://orcid.org/0000-0003-1704-0781
Hu Zou https://orcid.org/0000-0002-6684-3997

References

Abdul Karim, M., Aguilar, J., Ahlen, S., et al. 2025, PhRvD, 112, 083515
Adame, A. G., Aguilar, J., Ahlen, S., et al. 2025, JCAP, 2025, 028
Bayer, J., Huber, S., Vogl, C., et al. 2021, A&A, 653, A29
Bellm, E. C., Kulkarni, S. R., Graham, M. J., et al. 2019, PASP, 131, 018002
Bertin, E. 2006, ASPC, 351, 112
Bertin, E., & Arnouts, S. 1996, A&AS, 117, 393
Bertin, E., Mellier, Y., Radovich, M., et al. 2002, ASPC, 281, 228
Birrer, S., & Amara, A. 2018, PDU, 22, 189
Birrer, S., Shajib, A., Gilman, D., et al. 2021, JOSS, 6, 3283
Blagorodnova, N., Neill, J. D., Walters, R., et al. 2018, PASP, 130, 035003
Bushouse, H., Eisenhamer, J., Dencheva, N., et al. 2023, JWST Calibration Pipeline, v1.9.4, Zenodo, doi:10.5281/zenodo.7577320
Busmann, M., O'Connor, B., Sommer, J., et al. 2025, A&A, 701, A225
Byler, N., Dalcanton, J. J., Conroy, C., & Johnson, B. D. 2017, ApJ, 840, 44
CASA Team, Bean, B., Bhatnagar, S., et al. 2022, PASP, 134, 114501
Chabrier, G. 2003, PASP, 115, 763
Chambers, K. C., Magnier, E. A., Metcalfe, N., et al. 2016, arXiv:1612.05560
Chen, W., Kelly, P. L., Frye, B. L., et al. 2024, ApJ, 970, 102
Conroy, C., & Gunn, J. E. 2010, ApJ, 712, 833
Conroy, C., Gunn, J. E., & White, M. 2009, ApJ, 699, 486
Conroy, C., White, M., & Gunn, J. E. 2010, ApJ, 708, 58
Coughlin, M. W., Bloom, J. S., Nir, G., et al. 2023, ApJS, 267, 31
Coulter, D. A., Larison, C., Pierel, J. D. R., et al. 2026, arXiv:2601.04156

Cristiani, S., Cupani, G., Trost, A., et al. 2024, MNRAS, 528, 6845
Dekany, R., Smith, R. M., Riddle, R., et al. 2020, PASP, 132, 038001
DESI Collaboration, Abareshi, B., Aguilar, J., et al. 2022, AJ, 164, 207
DESI Collaboration, Abdul-Karim, M., Adame, A. G., et al. 2026, AJ, 171, 285
DESI Collaboration, Aghamousa, A., Aguilar, J., et al. 2016, arXiv:1611.00037
Duev, D. A., Mahabal, A., Masci, F. J., et al. 2019, MNRAS, 489, 3582
Dux, F. 2024, JOSS, 9, 6775
Dye, S., Lawrence, A., Read, M. A., et al. 2018, MNRAS, 473, 5113
Ferland, G. J., Porter, R. L., van Hoof, P. A. M., et al. 2013, RMxAA, 49, 137
Feroz, F., Hobson, M. P., & Bridges, M. 2009, MNRAS, 398, 1601
Flewelling, H. A., Magnier, E. A., Chambers, K. C., et al. 2020, ApJS, 251, 7
Gaia Collaboration 2020, yCat, I/350
Gaia Collaboration, Brown, A. G. A., Vallenari, A., et al. 2021, A&A, 649, A1
Goldstein, D. A., & Nugent, P. E. 2016, ApJL, 834, L5
Goobar, A., Adamo, A., Andreoni, I., et al. 2023b, Measuring the Hubble constant with the next multiple-imaged lensed supernova, JWST Proposal. Cycle 2, ID. #3468
Goobar, A., Amanullah, R., Kulkarni, S. R., et al. 2017, Sci, 356, 291
Goobar, A., Johansson, J., Schulze, S., et al. 2023a, NatAs, 7, 1098
Goobar, A., Lemon, C., Johansson, J., et al. 2025, TNSAN, 201, 1
Gordon, K. D., Clayton, G. C., Decleir, M., et al. 2023, ApJ, 950, 86
Gössl, C. A., & Riffeser, A. 2002, A&A, 381, 1095
Graham, M. J., Kulkarni, S. R., Bellm, E. C., et al. 2019, PASP, 131, 078001
Guy, J., Bailey, S., Kremin, A., et al. 2023, AJ, 165, 144
Higson, E., Handley, W., Hobson, M., & Lasenby, A. 2019, S&C, 29, 891
Hinkle, J. 2025, TNSCR, 2025-2137, 1
Hu, L., Wang, L., Chen, X., & Yang, J. 2022, ApJ, 936, 157
Jiménez-Vicente, J., & Mediavilla, E. 2022, ApJ, 941, 80
Johansson, J., Goobar, A., Price, S. H., et al. 2021, MNRAS, 502, 510
Johansson, J., Perley, D. A., Goobar, A., et al. 2025, ApJL, 995, L17
Johnson, B. D., Leja, J., Conroy, C., & Speagle, J. S. 2021, ApJS, 254, 22
Jones, D. O., McGill, P., Manning, T. A., et al. 2024, arXiv:2410.17322
Kelly, P. L., Rodney, S. A., Treu, T., et al. 2015, Sci, 347, 1123
Kelly, P. L., Rodney, S., Treu, T., et al. 2023, Sci, 380, eabh1322
Kim, Y.-L., Rigault, M., Neill, J. D., et al. 2022, PASP, 134, 024505
Lang-Bardl, F., Bender, R., Goessl, C., et al. 2016, SPIE, 9908, 990844
Lantz, B., Aldering, G., Antilogus, P., et al. 2004, SPIE, 5249, 146
Leja, J., Carnall, A. C., Johnson, B. D., Conroy, C., & Speagle, J. S. 2019a, ApJ, 876, 3
Leja, J., Johnson, B. D., Conroy, C., van Dokkum, P. G., & Byler, N. 2017, ApJ, 837, 170
Leja, J., Johnson, B. D., Conroy, C., et al. 2019b, ApJ, 877, 140
Lemon, C., Courbin, F., More, A., et al. 2024, SSRv, 220, 23
Lindegren, L., Klioner, S. A., Hernández, J., et al. 2021, A&A, 649, A2
Magnier, E. A., Schlafly, E. F., Finkbeiner, D. P., et al. 2020, ApJS, 251, 6
Mahabal, A., Rebbapragada, U., Walters, R., et al. 2019, PASP, 131, 038002
Masci, F. J., Laher, R. R., Rusholme, B., et al. 2019, PASP, 131, 018003
Michalewicz, K., Millon, M., Dux, F., & Courbin, F. 2023, JOSS, 8, 5340
Miller, T. N., Doel, P., Gutierrez, G., et al. 2024, AJ, 168, 95
Mörtsell, E., Johansson, J., Dhawan, S., et al. 2020, MNRAS, 496, 3270
Oguri, M., & Marshall, P. J. 2010, MNRAS, 405, 2579
Pascale, M., Frye, B. L., Pierel, J. D. R., et al. 2025, ApJ, 979, 13
Patterson, M. T., Bellm, E. C., Rusholme, B., et al. 2019, PASP, 131, 018001
Perley, D. A. 2019, PASP, 131, 084503
Perley, R. A., Chandler, C. J., Butler, B. J., & Wrobel, J. M. 2011, ApJL, 739, L1
Perrin, M. D., Sivaramakrishnan, A., Lajoie, C.-P., et al. 2014, SPIE, 9143, 91433X
Pierel, J. D. R., Hayes, E. E., Millon, M., et al. 2026, ApJ, 998, 219
Poppett, C., Tyas, L., Aguilar, J., et al. 2024, AJ, 168, 245
Quimby, R. M., Werner, M. C., Oguri, M., et al. 2013, ApJL, 768, L20
Rauscher, B. J. 2024, PASP, 136, 015001
Refsdal, S. 1964, MNRAS, 128, 307
Rigault, M., Neill, J. D., Blagorodnova, N., et al. 2019, A&A, 627, A115
Schechter, P. L., & Wambsganss, J. 2002, ApJ, 580, 685
Schlafly, E. F., & Finkbeiner, D. P. 2011, ApJ, 737, 103
Schlafly, E. F., Kirkby, D., Schlegel, D. J., et al. 2023, AJ, 166, 259
Shajib, A. J., Vernardos, G., Collett, T. E., et al. 2024, SSRv, 220, 87
Skilling, J. 2004, AIPC, 735, 395
Skilling, J. 2006, BayAn, 1, 833
Skrutskie, M. F., Cutri, R. M., Stiening, R., et al. 2006, AJ, 131, 1163
Speagle, J. S. 2020, MNRAS, 493, 3132
Taubenberger, S., Acebron, A., Cañameras, R., et al. 2025, arXiv:2510.21694
Thompson, A. R., Clark, B. G., Wade, C. M., & Napier, P. J. 1980, ApJS, 44, 151
Tonry, J. L., Denneau, L., Heinze, A. N., et al. 2018, PASP, 130, 064505
Tucker, M. A., Shappee, B. J., Huber, M. E., et al. 2022, PASP, 134, 124502
van der Walt, S., Crellin-Quick, A., & Bloom, J. 2019, JOSS, 4, 1247
Vanzella, E., Castellano, M., Bergamini, P., et al. 2022, A&A, 659, A2
Vega-Ferrero, J., Diego, J. M., Miranda, V., & Bernstein, G. M. 2018, ApJL, 853, L31
Vernardos, G., Sluse, D., Pooley, D., et al. 2024, SSRv, 220, 14
Weisenbach, L., Collett, T., de Murieta, A. S., et al. 2024, MNRAS, 531, 4349
Williams, P. K. G., Clavel, M., Newton, E., & Ryzhkov, D. 2017, pwkit: Astronomical utilities in Python, Astrophysics Source Code Library, ascl:1704.001
Wright, E. L., Eisenhardt, P. R. M., Mainzer, A. K., et al. 2010, AJ, 140, 1868
Zhou, R., Newman, J. A., Mao, Y.-Y., et al. 2021, MNRAS, 501, 3309
Zimmerman, E. A., Irani, I., Chen, P., et al. 2024, Natur, 627, 759